Dynamic evolution of flow structures and viscosity during basaltic magma emplacement and crystallization in an upper-crustal sill

LeeAnn Srogi[1,1], Arianna Soldati[2], Tim Lutz[1], Nikolas Watson[1], and Meagen Pollock[3]

[1]West Chester University of Pennsylvania
[2]North Carolina State University
[3]College of Wooster

November 30, 2022

Abstract

An upper-crustal intrusive network in the 201.5 Ma, rift-related Central Atlantic Magmatic Province is exposed in the western Newark basin (PA, USA). Alpha-MELTS modeling was used to track magma evolution starting with initial pyroxene crystallization at depth (1000-500 MPa); plagioclase crystallized during ascent in the upper crust. For magma emplaced at 5-6 km depth (170 MPa), six MELTS models were generated to bracket different composition, H2O (1-3 wt.%), and crystallinity (28-49 vol.%). Corresponding magma viscosities evolved from 3 to 1624 Pa-sec (predicted using Giordano et. al 2008; Moitra and Gonnermann 2014). Detailed crystal mush structures in a diabase sill are revealed in a dimension stone quarry. Ubiquitous asymmetric modal layers a few mm thick comprising plag-rich layers (PRL, 75% modal plag) overlying more pyx-rich layers outline the tops of hundreds of dm-m scale flow lobes in the quarry. Tabular plag in PRL show shape-preferred orientations, tiling, and pressure shadows around larger pyx that resemble analog experiments on particle slurries and indicate flow with limited mechanical compaction. During magma emplacement, recursive interactions of propagation, sorting, and crystallization self-organized as flow lobes with plag entrained and aligned along lobe tops. Our calculations show plag separation can reduce bimodal suspension viscosity; a positive feedback likely enhanced by shear thinning and crystal alignments. EDS analyses and X-ray maps show that plag has oscillatory-zoned cores (An82-67) with patchy-zoned mantles (An67) filled in by An66-63. In PRL, plag are cemented together by An62-55; Na-rich rims occur next to qtz-Kspar pockets. By the end of cementation, PRL liquid volume was significantly reduced to 11-18% compared with 28-45% in overall magma based on MELTS models for An62-55 plag. Diabase suspension viscosity increased to >6000 Pa-sec; PRL viscosity cannot be modeled by equations based on random packing. PRL with aligned interlocking crystals were more rigid and less permeable than surrounding diabase. Upward flow of magma after modal layer development was channelized into pipes truncated and deflected by PRL. Thus, lateral flow during emplacement developed sub-vertical heterogeneities that exemplify complex mush rheology over m-scale distances.

Dynamic evolution of flow structures and viscosity during basaltic magma emplacement and crystallization in an upper-crustal sill

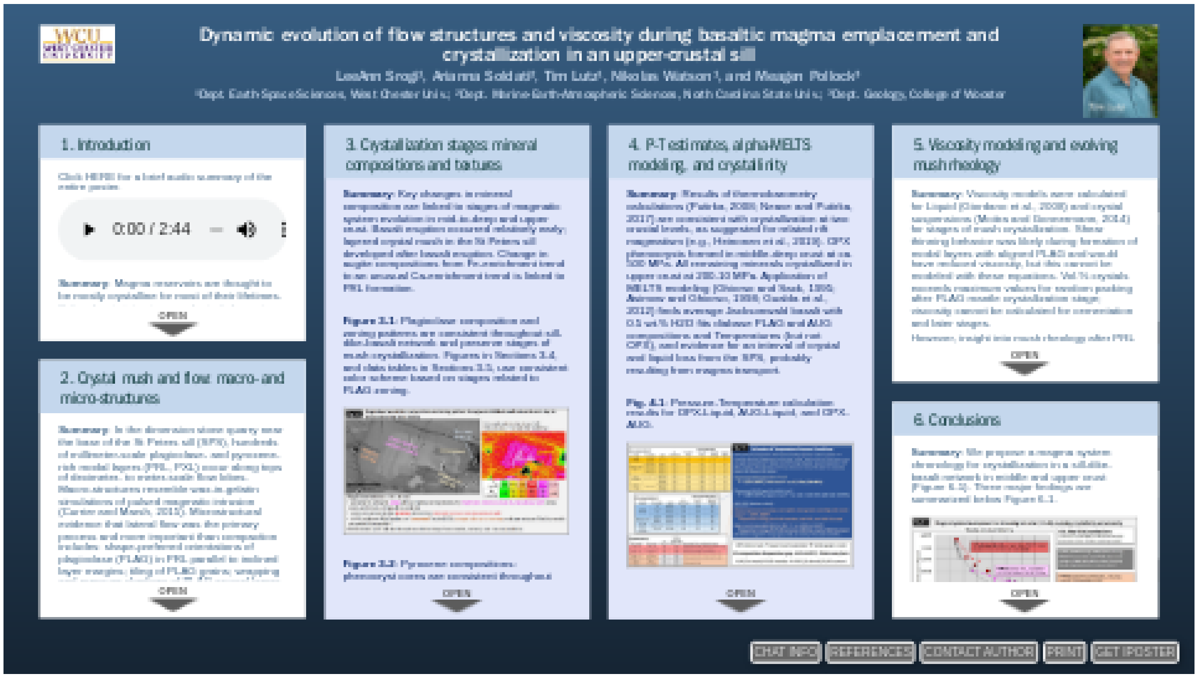

LeeAnn Srogi[1], Arianna Soldati[2], Tim Lutz[1], Nikolas Watson[1], and Meagen Pollock[3]

[1]Dept. Earth-Space Sciences, West Chester Univ.; [2]Dept. Marine-Earth-Atmospheric Sciences, North Carolina State Univ.; [3]Dept. Geology, College of Wooster

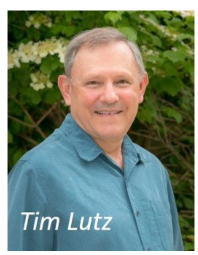

PRESENTED AT:

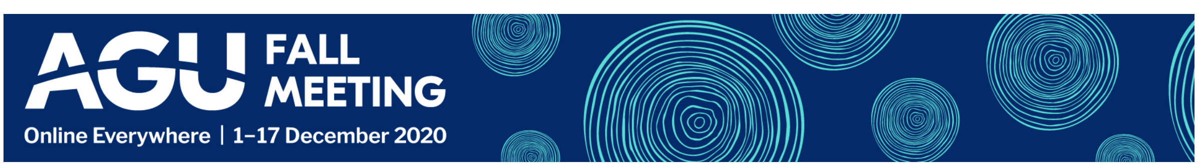

1. INTRODUCTION

Click HERE for a brief audio summary of the entire poster.

Summary: Magma reservoirs are thought to be mostly crystalline for most of their lifetimes. Sub-volcanic intrusions are logical places to study crystal mushes, but plutonic rocks are overprinted and incomplete records that need to be interpreted within the context of an entire magmatic system. We find an appropriate upper-crustal magma system comprising a sill-dike network from basalt down to a sill intruded at 5.5-6 km (Section 1). The network is part of the 201.5 Ma Central Atlantic Magmatic Province (CAMP), a global-scale magmatic event associated with rifting of Pangaea.

This poster focuses on solidified basaltic crystal mush (***diabase = dolerite = gabbro***) in an upper-crustal sill and associated sub-volcanic plumbing system. A general history of the magmatic system, and evolution of mush composition and rheology during crystallization, are developed using field evidence (Sections 2 and 5), mineral compositions and petrography (Section 3), P-T estimates and thermodynamic modeling (Section 4), and crystallinity estimates and viscosity modeling (Sections 4-5).

Figure 1-1: Maps and information about the Central Atlantic Magmatic Province in Eastern North America and the study area in the Newark basin.

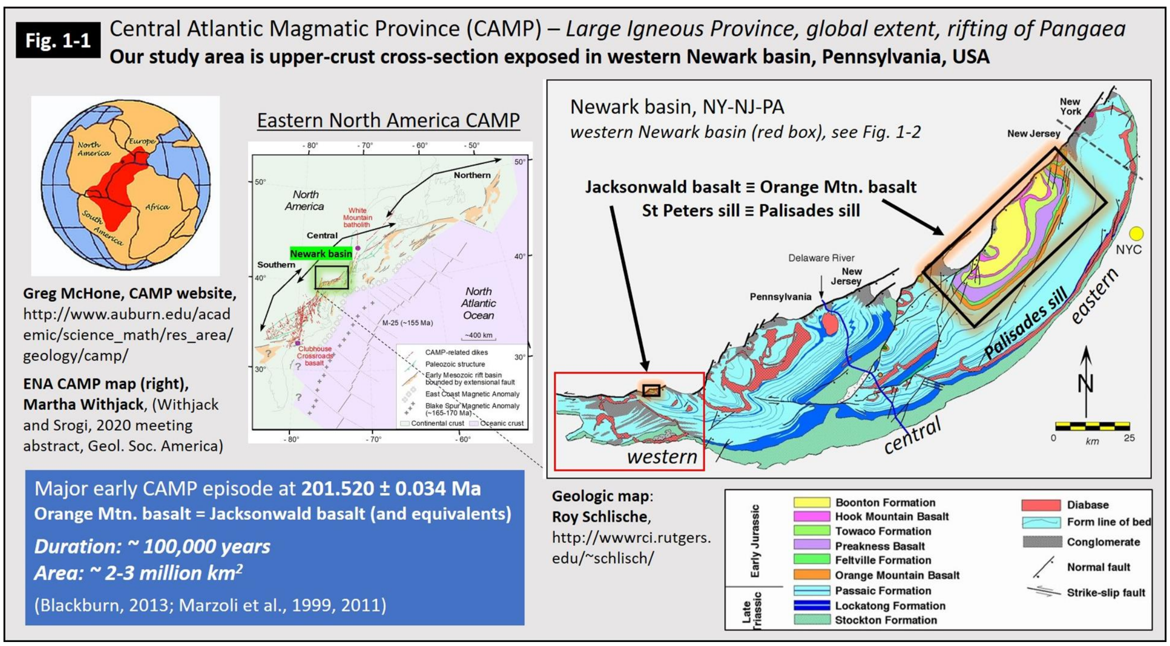

Figure 1-2: Maps and cross-sections showing the entire upper-crust sill-dike network exposed in the western Newark basin, and the St Peters sill comprising the crystal mush that is the focus of this poster.

Fig. 1-2 **Morgantown-Jacksonwald Intrusive Complex, western Newark basin**

Study location: St Peters sill, intruded at 5.5-6 km depth

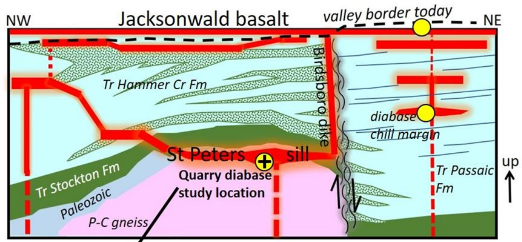

Dimension stone quarry near base of St Peters sill, Elverson, PA, USA

Geologic units from USGS on Google Earth base map

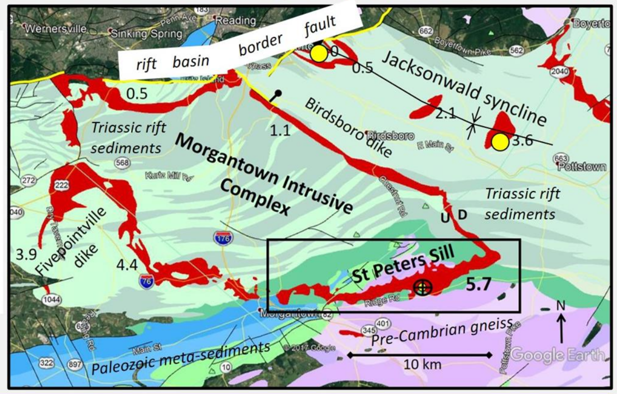

Erosion and post-magmatic tilting towards border fault exposes **complete cross-section of sill-dike network** from **Jacksonwald basalt** at paleo-surface *(next to border fault, Jacksonwald syncline)* to **St Peters sill** that intruded basement at 5.5-6 km paleo-depth *(numbers on map above, paleo-depth estimates; Srogi et al., 2017)*.

Upper left: **Schematic cross-section looking NNW**, minimal vertical exaggeration. Yellow circles are sample locations referenced on this poster, including **dimension stone quarry in St Peters sill (*bottom left*)** that is main focus of this poster.

2. CRYSTAL MUSH AND FLOW: MACRO- AND MICRO-STRUCTURES

Summary: In the dimension stone quarry near the base of the St Peters sill (SPS), hundreds of millimeter-scale plagioclase- and pyroxene-rich modal layers (PRL, PXL) occur along tops of decimeter- to meter-scale flow lobes. Macro-structures resemble wax-in-gelatin simulations of pulsed magmatic intrusion (Currier and Marsh, 2015). Microstructural evidence that lateral flow was the primary process and more important than compaction includes: shape-preferred orientations of plagioclase (PLAG) in PRL parallel to inclined layer margins; tiling of PLAG grains; wrapping and pressure shadows of PLAG around larger pyroxene (PX) grains within PRL. Microstructures resemble spindle viscometer experiments using bimodal analog particle slurries (Cimarelli et al., 2011).

Figure 2-1: Location and information about dimension stone quarry near base of SPS. The quarry measures roughly 60m x 50m, with a total of about 20m vertical exposure.

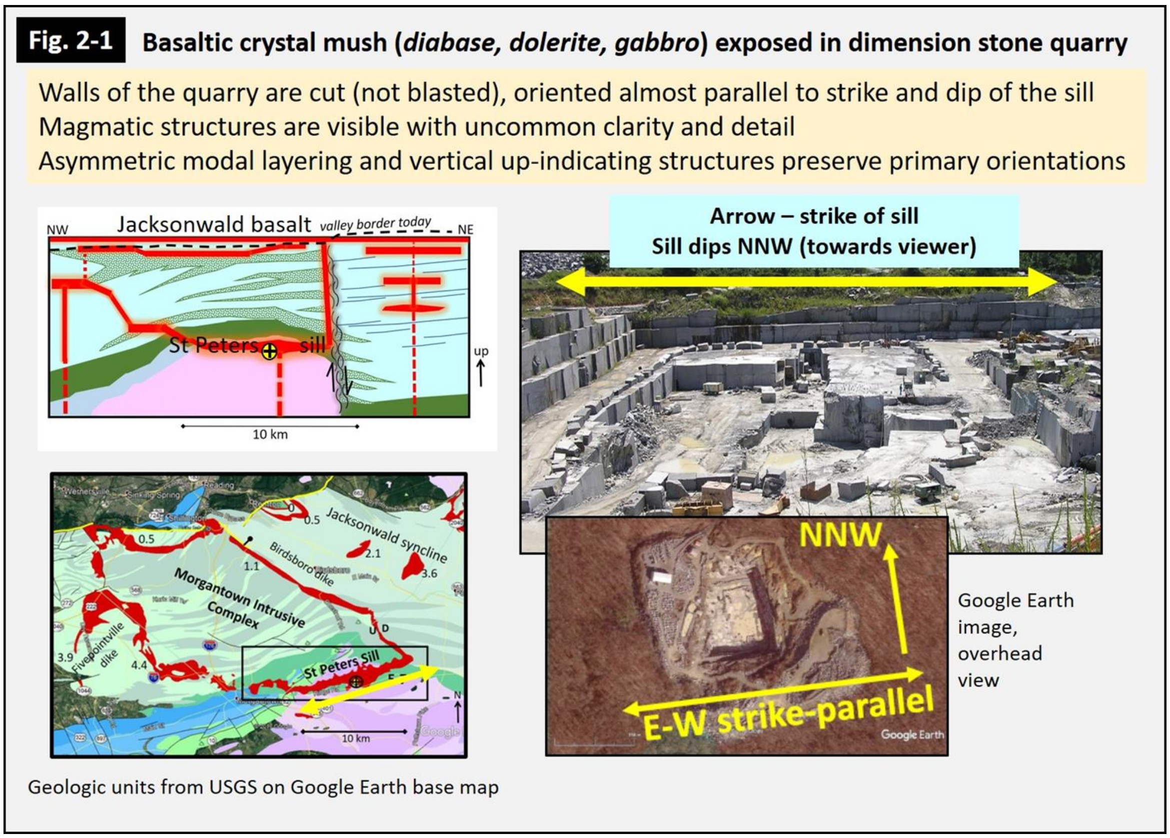

Figure 2-2: Macro-structures - plagioclase-rich layers (PRL) and flow lobes - in diabase crystal mush in the SPS dimension stone quarry, viewed on wall cut parallel to strike of sill, normal to dip of PRL.

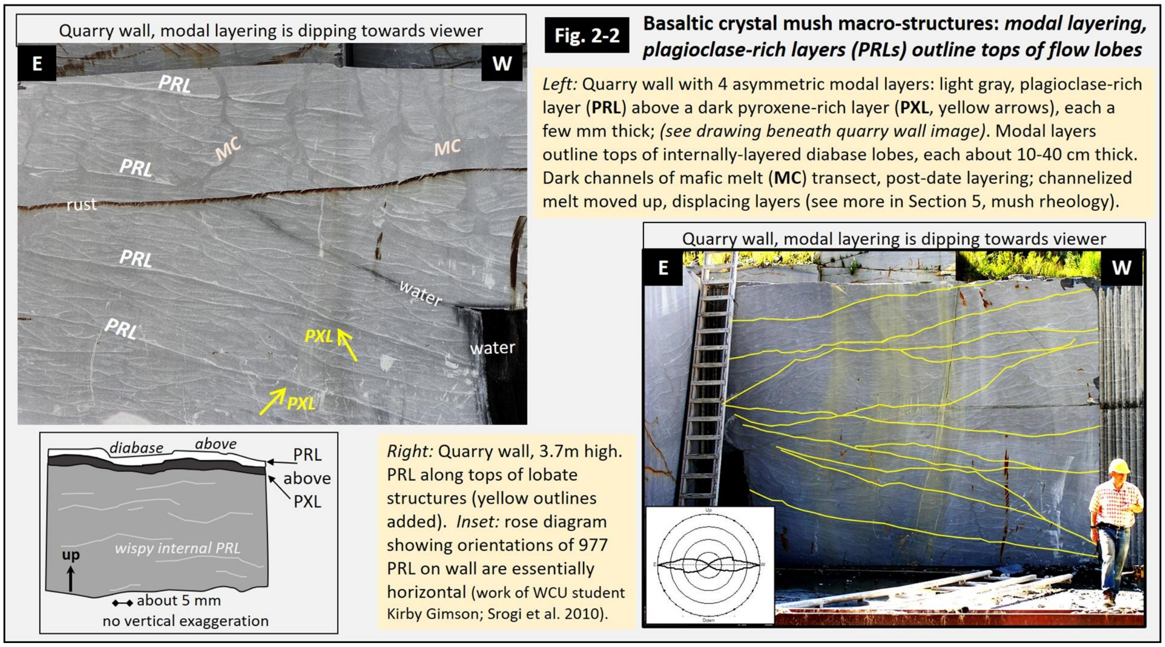

Figure 2-3: Flow lobes viewed on wall cut normal to sill strike and parallel to PRL dip; and on block surface cut at shallow angle (about 20º) to PRL dip. Latter section shows overlapping lobes similar to wax-in-gelatin models of pulsed magmatic flow (Currier and Marsh, 2015). This link may take you to the wax model videos; note especially Videos 3 and 5: Link to videos of wax models, Currier and Marsh (2015) (http://dx.doi.org/10.1016/j.jvolgeores.2015.07.009)

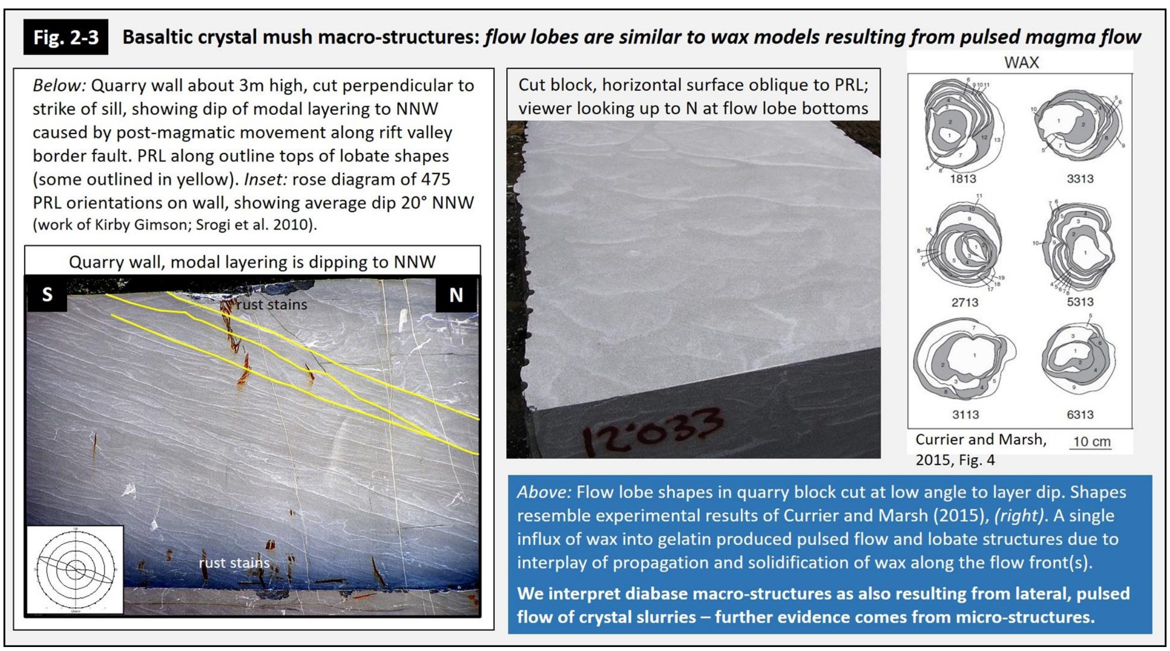

Figure 2-4: Orientation of thin section for viewing and measuring micro-structures in the PRL.

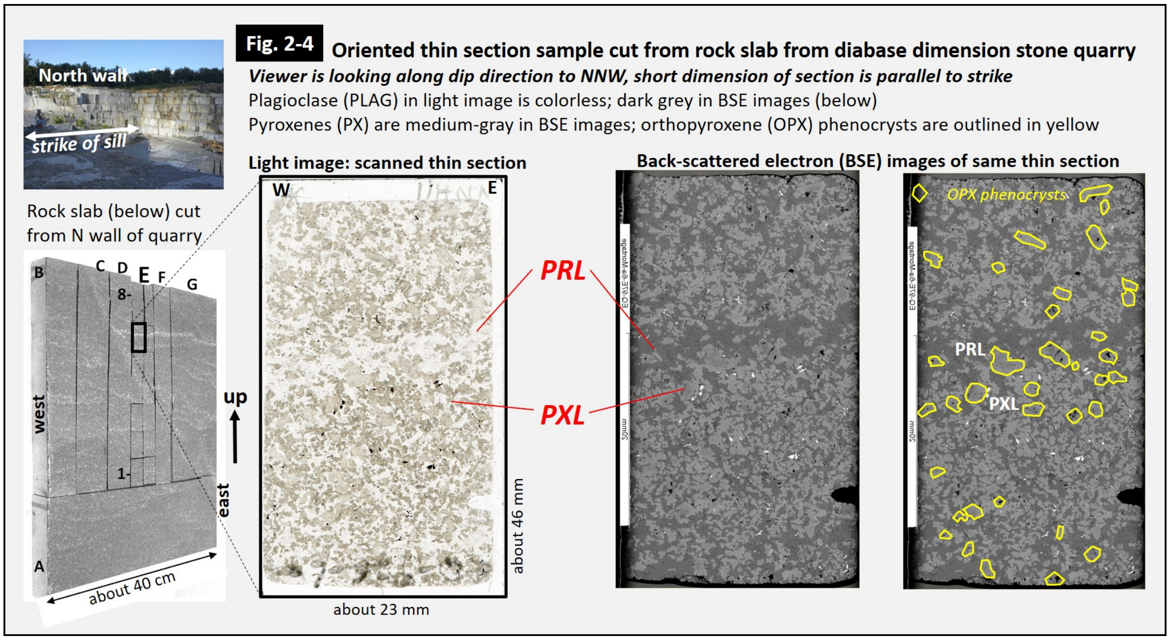

Figure 2-5: Plagioclase-rich layer (PRL) viewed in thin section (cross-polarized light) showing shape-preferred orientations of PLAG.

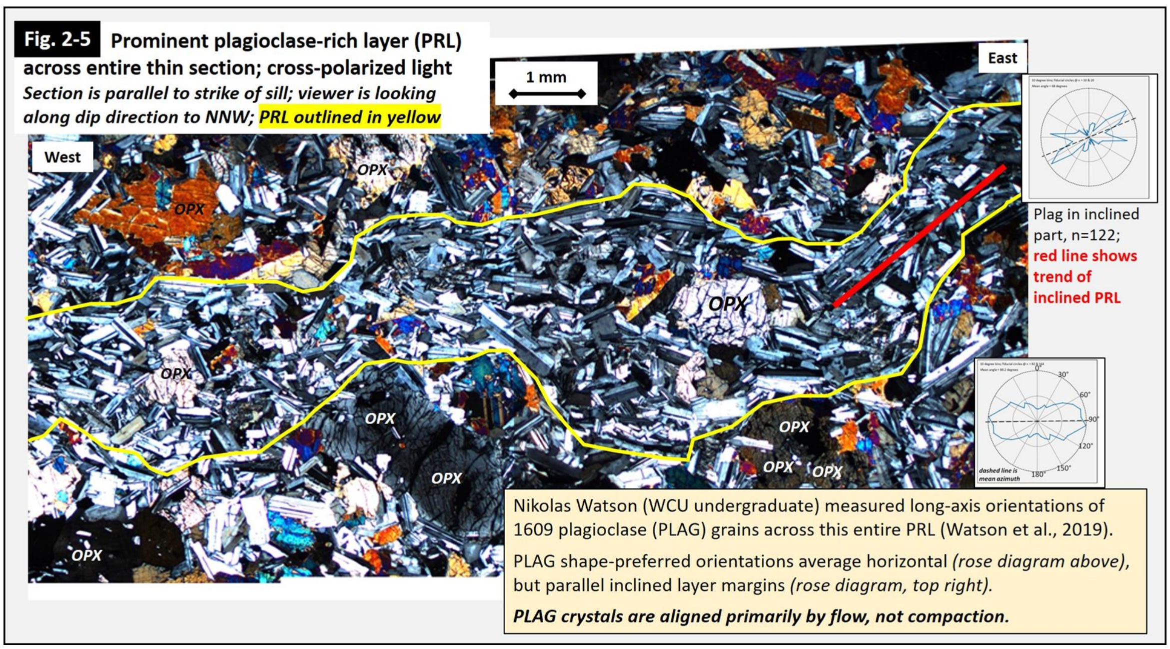

Figure 2-6: Micro-structural evidence for flow in PRL, similar to structures in analog experiments in bimodal slurries resulting from shear flow and shear thinning (Cimarelli et al., 2011).

Fig. 2-6 **Micro-structures in 3 perpendicular thin sections indicate shear flow within PRL**

Flow structures are similar to analog viscometer experiments on bimodal crystal slurries by Cimarelli et al. (2011): shear flow and shear thinning caused separation of small fibers (=PLAG) from larger spheres (=OPX), and flow alignment of fibers

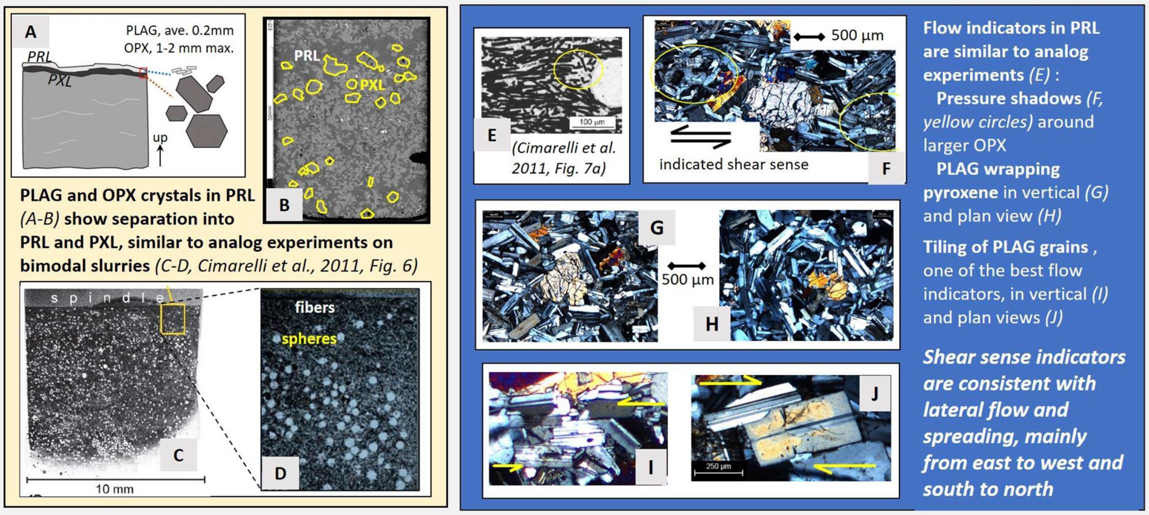

3. CRYSTALLIZATION STAGES: MINERAL COMPOSITIONS AND TEXTURES

Summary: Key changes in mineral composition are linked to stages of magmatic system evolution in mid-to-deep and upper crust. Basalt eruption occurred relatively early; layered crystal mush in the St Peters sill developed after basalt eruption. Change in augite compositions from Fe-enrichment trend to an unusual Ca-enrichment trend is linked to PRL formation.

Figure 3-1: Plagioclase composition and zoning patterns are consistent throughout sill-dike-basalt network and preserve stages of mush crystallization. Figures in Sections 3-4, and data tables in Sections 3-5, use consistent color scheme based on stages related to PLAG zoning.

Fig. 3-1 **Plagioclase has similar composition and zoning pattern throughout sill-dike-basalt network and is key to interpreting magmatic history**

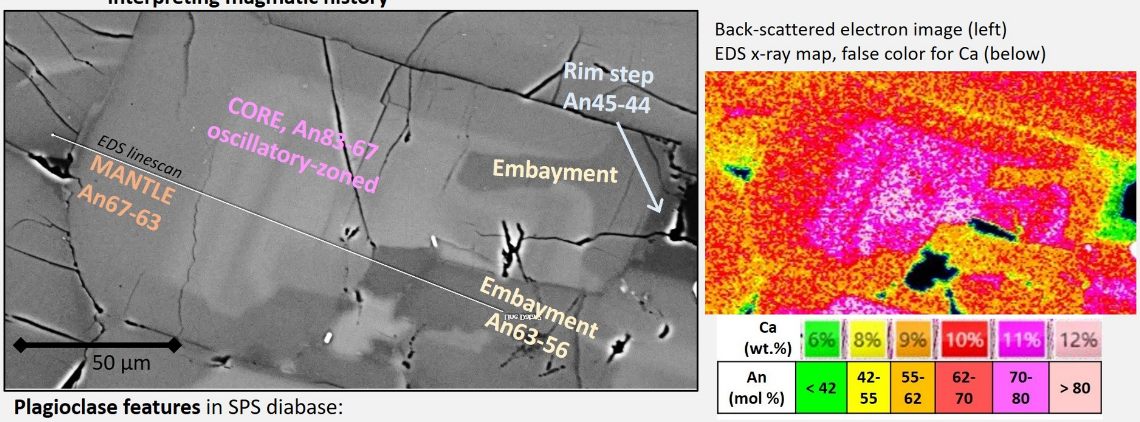

Plagioclase features in SPS diabase:

- euhedral to anhedral ***cores*** with oscillatory zoning (An83-67); bright pink colors on Ca x-ray map above right; some cores are broken, embayed (resorption)
- cores are surrounded by ***mantles*** of An67-63; red color on Ca x-ray map above right
- in PRL, adjacent PLAG grains are "***cemented***" by An63-56; orange colors on x-ray map; embayments are filled by mantle or cement composition

EDS linescans (not included here) show distinct steps from mantle, cement, and rim compositions

Figure 3-2: Pyroxene compositions: phenocryst cores are consistent throughout sill-dike-basalt network; 2 trends are identified for augite (AUG).

Fig. 3-2 **Pyroxene compositions in the SPS, basalt, and a diabase chill margin**

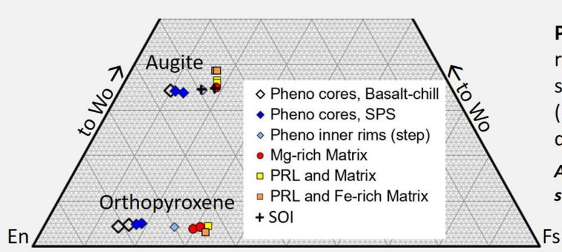

Pyroxene compositions recalculated using scheme of Lindsley (1983), plotted on quadrilateral diagram

All data for SPS except some Phenocryst cores

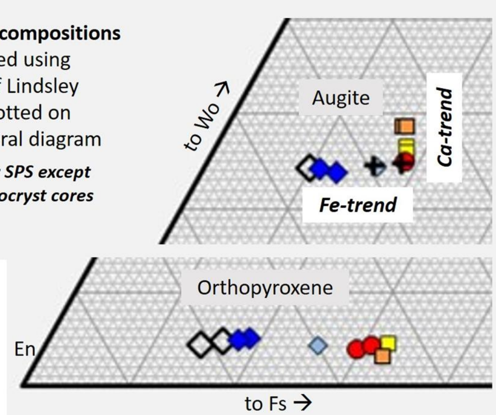

SPS: St Peters sill; PRL: Plagioclase-rich layer; SOI: AUG-PLAG sub-ophitic intergrowth

OPX and AUG show normal ***Fe-trend*** of increasing Fs component (increasing Fe) from phenocryst cores to sub-ophitic AUG-PLAG intergrowths to most Mg-rich matrix grains.

***Ca-trend* in AUG**, increasing Wo component with same or increasing Mg#, is not predicted by models of 2-pyroxene fractionation.

Figure 3-3: Similar early-formed crystal cargo in Jacksonwald basalt and St Peters sill demonstrates volcanic-plutonic link and relative timing of eruption(s) in history of this magma system.

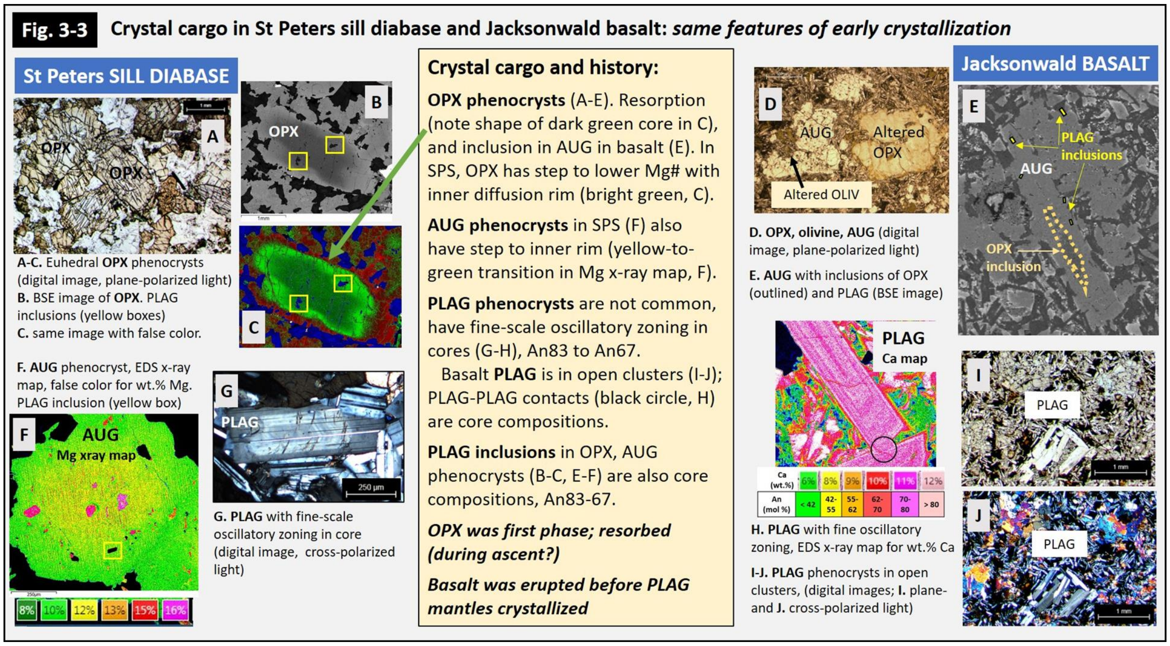

Figure 3-4: During and after eruption(s) came an active interval of multiple resorption and recharge events. Crystallization resumed with growth of plagioclase mantles and augite following the Fe-enrichment trend.

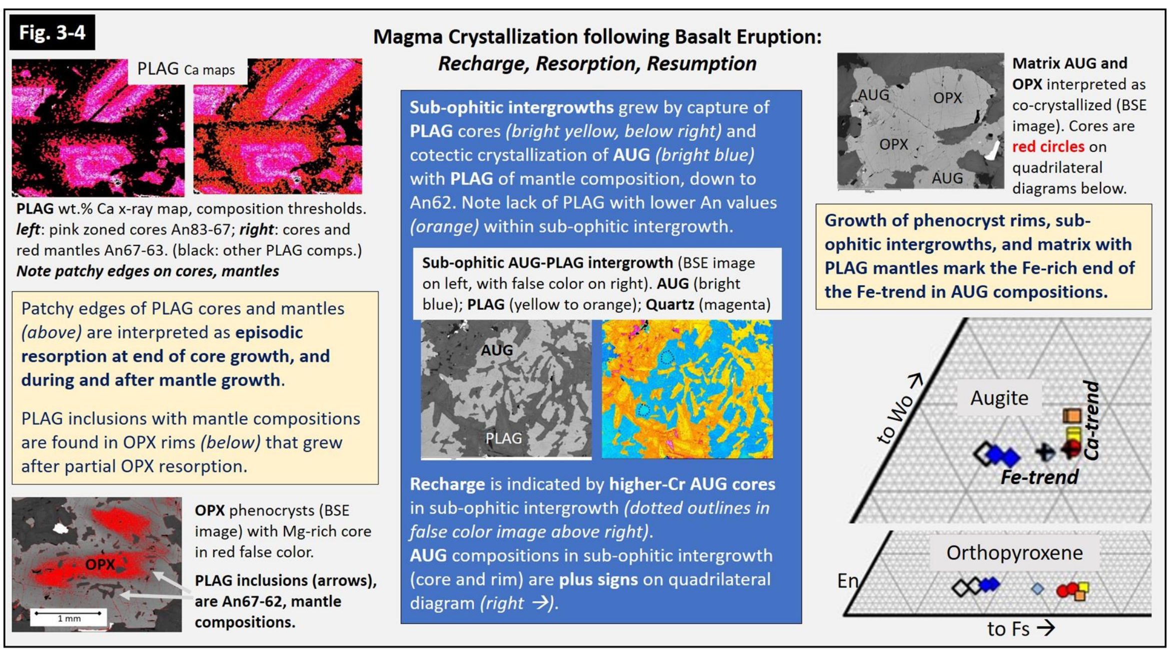

Figure 3-5: Ca x-ray maps with composition thresholds show the progressive growth of plagioclase in 4 areas of a plagioclase-rich layer (PRL). Timing of PLAG alignment and PRL formation is identified: after PLAG mantles and before cementation of the PRL.

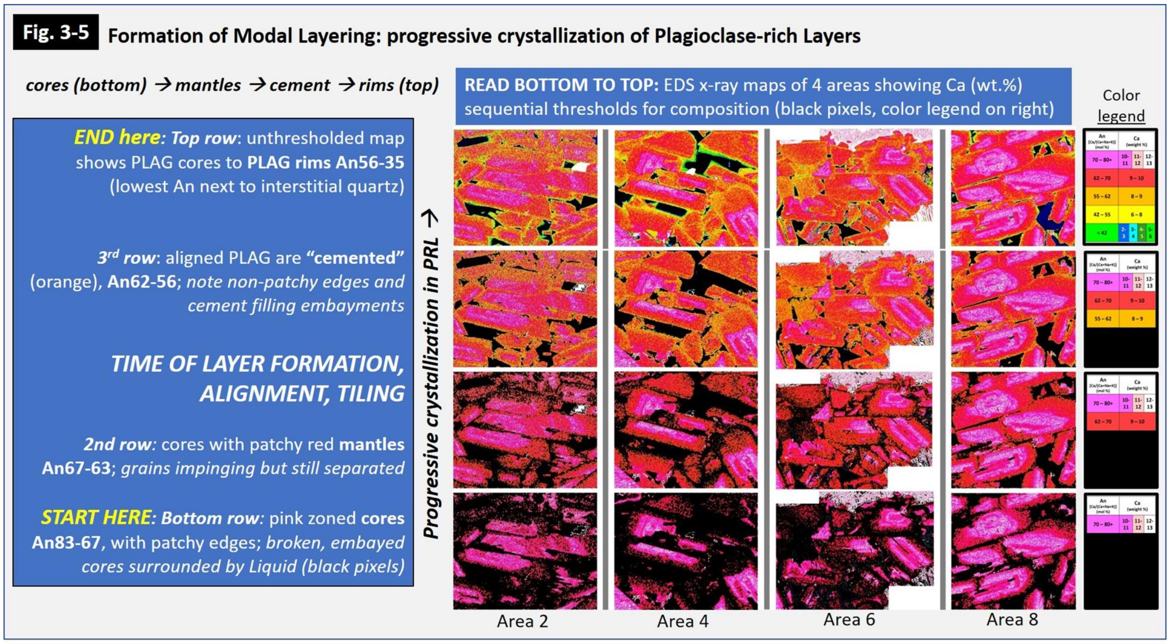

Figure 3-6: Augite associated with the PLAG cement composition and later minerals follow the Ca-enrichment trend. Formation of the PRL seems to mark a shift in crystal-Liquid equilibria.

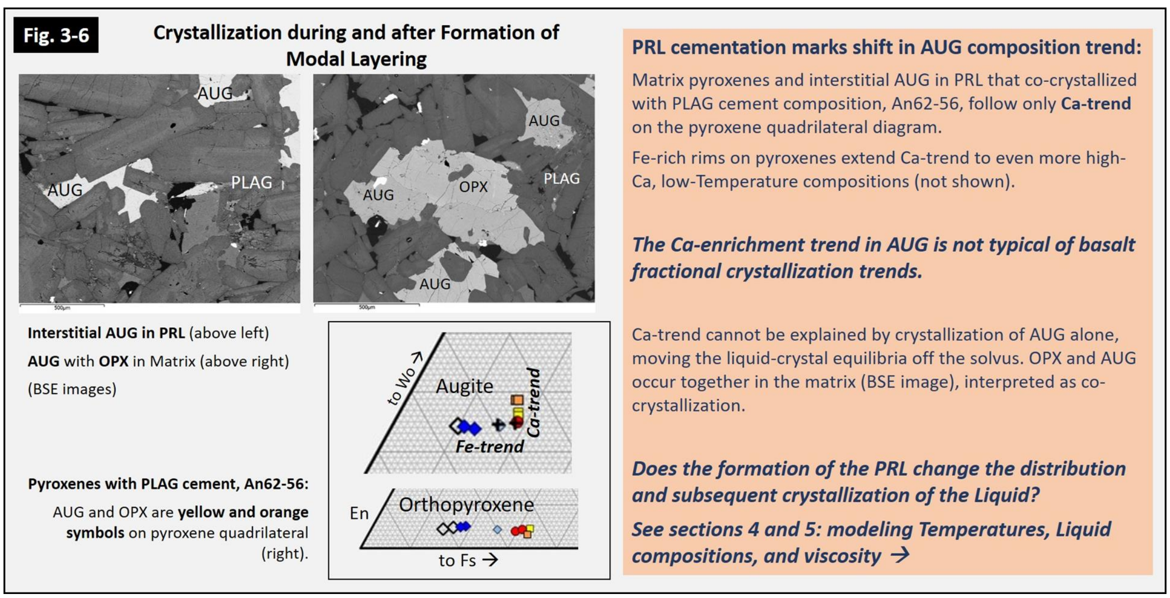

4. P-T ESTIMATES, ALPHA-MELTS MODELING, AND CRYSTALLINITY

Summary: Results of thermobarometry calculations (Putirka, 2008; Neave and Putirka, 2017) are consistent with crystallization at two crustal levels, as suggested for related rift magmatism (e.g., Heinonen et al., 2019). OPX phenocrysts formed in middle-deep crust at ca. 500 MPa. All remaining minerals crystallized in upper crust at 200-10 MPa. Application of MELTS modeling (Ghiorso and Sack, 1995; Asimow and Ghiorso, 1998; Gualda et al., 2012) finds average Jacksonwald basalt with 0.5 wt.% H2O fits diabase PLAG and AUG compositions and Temperatures (but not OPX), and evidence for an interval of crystal and liquid loss from the SPS, probably resulting from magma transport.

Fig. 4-1: Pressure-Temperature calculation results for OPX-Liquid, AUG-Liquid, and OPX-AUG.

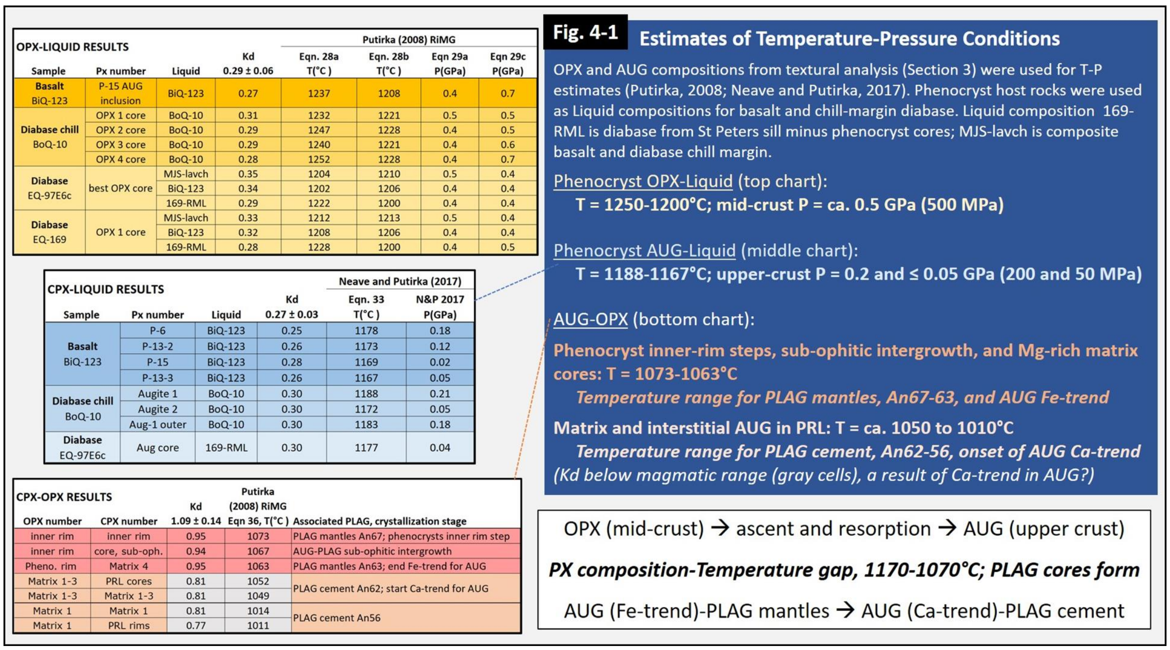

OPX-LIQUID RESULTS

Sample	Px number	Liquid	Kd 0.29 ± 0.06	Putirka (2008) RiMG Eqn. 28a T(°C)	Eqn. 28b T(°C)	Eqn 29a P(GPa)	Eqn 29c P(GPa)
Basalt BiQ-123	P-15 AUG inclusion	BiQ-123	0.27	1237	1208	0.4	0.7
Diabase chill BoQ-10	OPX 1 core	BoQ-10	0.31	1232	1221	0.5	0.5
	OPX 2 core	BoQ-10	0.29	1247	1228	0.4	0.5
	OPX 3 core	BoQ-10	0.29	1240	1221	0.4	0.6
	OPX 4 core	BoQ-10	0.28	1252	1228	0.4	0.7
Diabase EQ-97E6c	best OPX core	MJS-lavch	0.35	1204	1210	0.5	0.4
		BiQ-123	0.34	1202	1206	0.4	0.4
		169-RML	0.29	1222	1200	0.4	0.4
Diabase EQ-169	OPX 1 core	MJS-lavch	0.33	1212	1213	0.5	0.4
		BiQ-123	0.32	1208	1206	0.4	0.4
		169-RML	0.28	1228	1200	0.4	0.5

CPX-LIQUID RESULTS

Sample	Px number	Liquid	Kd 0.27 ± 0.03	Neave and Putirka (2017) Eqn. 33 T(°C)	N&P 2017 P(GPa)
Basalt BiQ-123	P-6	BiQ-123	0.25	1178	0.18
	P-13-2	BiQ-123	0.26	1173	0.12
	P-15	BiQ-123	0.28	1169	0.02
	P-13-3	BiQ-123	0.26	1167	0.05
Diabase chill BoQ-10	Augite 1	BoQ-10	0.30	1188	0.21
	Augite 2	BoQ-10	0.30	1172	0.05
	Aug-1 outer	BoQ-10	0.30	1183	0.18
Diabase EQ-97E6c	Aug core	169-RML	0.30	1177	0.04

CPX-OPX RESULTS

OPX number	CPX number	Kd 1.09 ± 0.14	Putirka (2008) RiMG Eqn 36, T(°C)	Associated PLAG, crystallization stage
inner rim	inner rim	0.95	1073	PLAG mantles An67; phenocrysts inner rim step
inner rim	core, sub-oph.	0.94	1067	AUG-PLAG sub-ophitic intergrowth
Pheno. rim	Matrix 4	0.95	1063	PLAG mantles An63; end Fe-trend for AUG
Matrix 1-3	PRL cores	0.81	1052	PLAG cement An62; start Ca-trend for AUG
Matrix 1-3	Matrix 1-3	0.81	1049	
Matrix 1	Matrix 1	0.81	1014	PLAG cement An56
Matrix 1	PRL rims	0.77	1011	

Fig. 4-1 Estimates of Temperature-Pressure Conditions

OPX and AUG compositions from textural analysis (Section 3) were used for T-P estimates (Putirka, 2008; Neave and Putirka, 2017). Phenocryst host rocks were used as Liquid compositions for basalt and chill-margin diabase. Liquid composition 169-RML is diabase from St Peters sill minus phenocryst cores; MJS-lavch is composite basalt and diabase chill margin.

Phenocryst OPX-Liquid (top chart):
T = 1250-1200°C; mid-crust P = ca. 0.5 GPa (500 MPa)

Phenocryst AUG-Liquid (middle chart):
T = 1188-1167°C; upper-crust P = 0.2 and ≤ 0.05 GPa (200 and 50 MPa)

AUG-OPX (bottom chart):
Phenocryst inner-rim steps, sub-ophitic intergrowth, and Mg-rich matrix cores: T = 1073-1063°C
Temperature range for PLAG mantles, An67-63, and AUG Fe-trend
Matrix and interstitial AUG in PRL: T = ca. 1050 to 1010°C
Temperature range for PLAG cement, An62-56, onset of AUG Ca-trend
(Kd below magmatic range (gray cells), a result of Ca-trend in AUG?)

OPX (mid-crust) → ascent and resorption → AUG (upper crust)
PX composition-Temperature gap, 1170-1070°C; PLAG cores form
AUG (Fe-trend)-PLAG mantles → AUG (Ca-trend)-PLAG cement

Figure 4-2: A total of 35 alpha-MELTS models (Ghiorso and Sack, 1995; Asimow and Ghiorso, 1998; Gualda et al., 2012) were run: average Jacksonwald basalt Liquid AB3 with 0.5 wt.% H2O fits the diabase PLAG and AUG compositions and Temperatures (but not OPX).

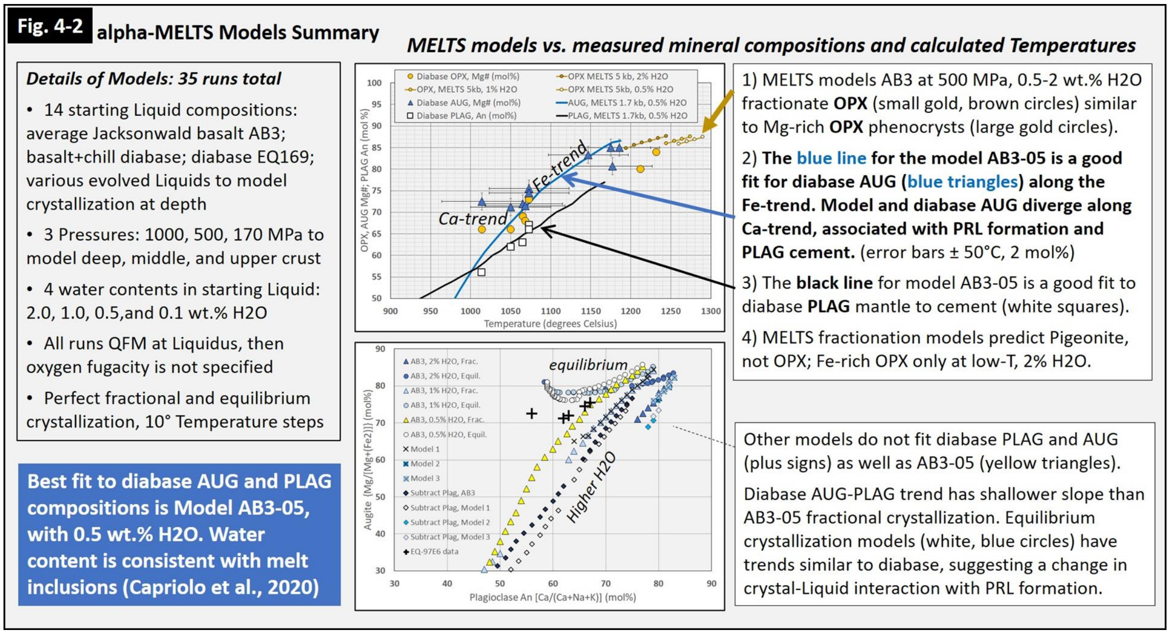

Figure 4-3: MELTS model AB3 predicts 30-35 vol.% pyroxenes crystallized in the interval between pyroxene cores and matrix (Temp. = 1170-1070ºC). However, diabase contains only 5-8 vol.% pyroxenes with these compositions. Magma transport and eruption during this interval would explain "missing" pyroxenes and be consistent with textural evidence from PLAG cores which were forming at that time.

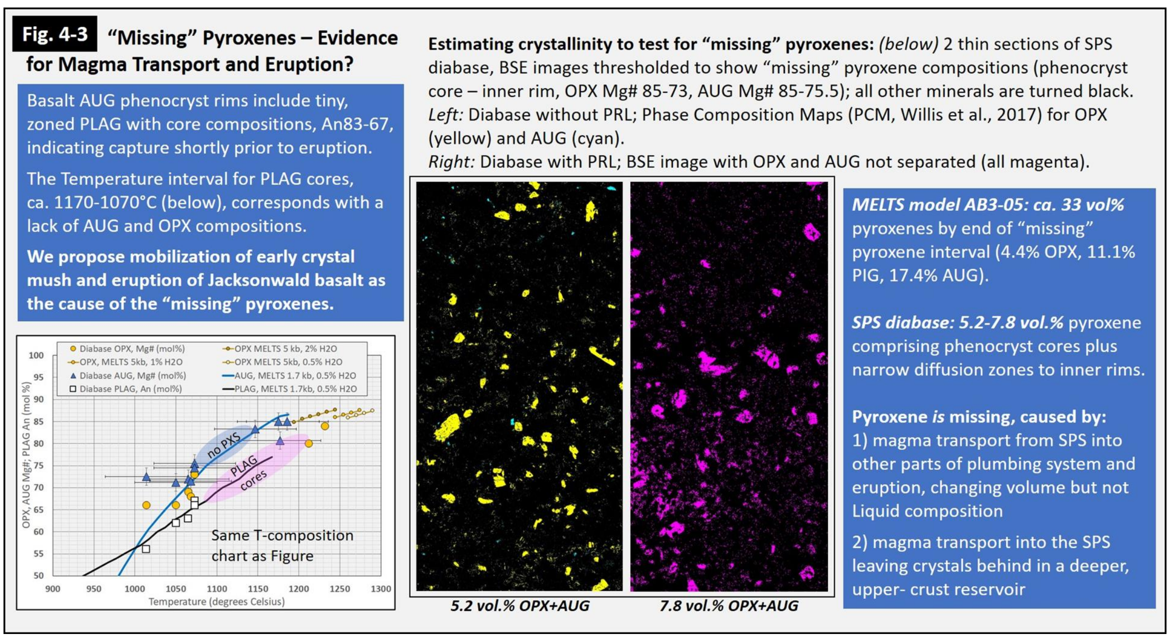

Figure 4-4: Estimates of volume % crystals in diabase and PRL from sample images and MELTS models.

Fig. 4-4 **Crystallinity must be estimated before using a viscosity model for crystal suspensions**

Stages of crystallization identified from composition-texture analysis, P-T estimates, MELTS models.

Jacksonwald basalt AB3 used as initial Liquid composition and as starting Liquid in all MELTS models shown here.

Vol.% crystals estimated from MELTS uses model output: Liquid composition, fractionated mineral mass and density.

Vol.% crystals estimated from diabase samples and PRL based on thresholding BSE images in ImageJ for mineral compositions corresponding with stages in crystallization history.

- Best estimates come from the diabase Phase Composition Maps, which are BSE images calibrated by EDS analyses and processed to generate separate images for PLAG, OPX, and AUG (Willis et al., 2017). Diabase PCM does not include a PLAG-rich layer (PRL).
- Vol.% crystals in diabase with PRL and the entire PLAG-rich layer (across the thin section) estimated by thresholding BSE image of all minerals using PCM images and thresholds as a guide.
- Vol.% crystals in the 4 areas of the PRL (see Figure 3-5) estimated by thresholding Ca x-ray maps for PLAG composition.

Crystalllinity (volume % crystals) for MELTS models, Diabase samples, PRLs

Stage in crystallization history	MELTS AB3 1.0 wt.% H2O			MELTS AB3 0.5 wt.% H2O			Diabase PCM no PRL			Diabase BSE with PRL			PRL entire PLAG+PXS			PRL 4 areas PLAG only		
	PXS	**PLAG**	**Total**	**PXS**	**PLAG**	**Total**	**PXS**	**PLAG**	**Total**	**PXS**	**PLAG**	**Total**	**PXS**	**PLAG**	**Total**	**PXS**	**PLAG**	**Total**
Liquidus, 500 MPa	0	0	0.0	0	0	0.0							*no PRL at these stages*			*no PRL at these stages*		
after OPX crystals, 500 MPa	4.0	0	4.0	4.3	0	4.3	4.9	0	4.9	4.9	0	4.9						
ascent, resorption, 170 MPa	4.0	0	4.0	4.0	0	4.0	2.5	0	2.5	2.5	0	2.5						
erupted basalt, AUG Mg83.5	22.6	4.0	26.6	22.2	8.8	31.0												
after PLAG cores, An83-67	*MELTS model not good fit*			32.9	18.61	51.5	5.2	18.4	23.6	7.8	19.6	27.3						
after PLAG mantles, An67-63				37.0	26.7	63.7	12.7	29.6	42.4	20.4	31.3	51.8	11.6	46.8	58.4	0.0	63.9	63.9
after PLAG cement, An63-56				39.2	31.1	70.3	36.9	39.7	76.6	39.0	44.3	83.3	20.2	67.6	87.8	0.0	86.9	86.9

5. VISCOSITY MODELING AND EVOLVING MUSH RHEOLOGY

Summary: Viscosity models were calculated for Liquid (Giordano et al., 2008) and crystal suspensions (Moitra and Gonnermann, 2014) for stages of mush crystallization. Shear thinning behavior was likely during formation of modal layers with aligned PLAG and would have reduced viscosity, but this cannot be modeled with these equations. Vol.% crystals exceeds maximum values for random packing after PLAG mantle crystallization stage; viscosity cannot be calculated for cementation and later stages.

However, insight into mush rheology after PRL formation and cementation comes from macro-structures in the diabase quarry. Increased viscosity and rigidity of crystal mush changed intrusive style of younger magma inputs from lateral sheet flow to channelized vertical flow.

Figure 5-1: Calculated viscosity and consistency results for Liquid and crystal suspensions, respectively.

Stage in crystallization history	Source of Vol.% crystal data	Temp. (°C)	H_2O in Liquid (wt.%)	Volume % and type of crystals (pyroxene, Px; plagioclase, Pl)	Volume % Liquid	Liquid Viscosity (Pa-sec)	Suspension consistency (K, Pa-sec)
Liquidus before crystallization	AB3, 500 MPa	1290	0.5	0	100	6.601	6.601
	AB3, 500 MPa	1274	1.0	0	100	5.361	5.361
after OPX crystallization at depth	Diabase	1260	0.53	4.9 Px	95.1	10.04	12.03
	Diabase	1243	1.04	4.9 Px	95.1	8.012	9.596
	AB3, 500 MPa	1260	0.53	4.3 Px	95.7	10.04	11.75
	AB3, 500 MPa	1244	1.04	4.0 Px	96.0	8.012	9.272
after ascent, OPX partial resorption	Diabase	1227	0.5	2.5 Px	97.5	15.46	16.92
	Diabase	1212	1.0	2.5 Px	97.5	11.26	12.32
	AB3, 170 MPa	1227	0.5	4 Px	96.0	15.46	17.89
	AB3, 170 MPa	1217	1.0	4 Px	96.0	11.26	13.03
basalt, based on AUG Mg# 83.5	AB3, 170 MPa	1147	0.76	22.2Px + 8.8Pl	69	67.01	268.2
	AB3, 170 MPa	1117	1.44	22.6Px + 4Pl	73.4	62.62	193.1
after crystalln. of PLAG cores, PX cores, inner rims	Diabase w/PRL	1073	1.48	7.8Px + 19.6Pl	72.0	470.9	1519
	Diabase no PRL	1073	1.48	5.2Px + 18.4Pl	75.5	470.9	1236
	AB3, 170 MPa	1087	1.19	32.9Px + 21.2Pl	45.7	274.6	12537
no PRL at this stage	*PRL entire*	*1073*	*1.48*	*4.0Px + 26.4Pl*	*69.6*	*470.9*	*1815*
	PRL 4-area med.	*1073*	*1.48*	*34.4 Plag*	*65.7*	*470.9*	*332253*
after crystallization of PLAG mantles, An67-63; AUG Fe-trend	Diabase w/PRL	1065	2.20	20.4Px + 31.3Pl	47.7	1131	33724
	Diabase no PRL	1065	2.20	12.7Px + 29.6Pl	57.0	1131	10742
	AB3, 170 MPa	1047	1.63	37Px + 26.7Pl	34.8	1131	4.89E+06
	PRL entire	1065	2.20	11.6Px + 46.8Pl	41.6	1131	151065
	PRL 4-area med.	1065	2.20	63.9 Plag	36.1	1131	*exceeds phi*
after crystallization of PLAG cement, An63-56; AUG Ca-trend	Diabase w/PRL	1014	3.50	39Px + 44.3Pl	16.5	4141	*exceeds phi*
	Diabase no PRL	1014	3.50	36.9Px + 39.7Pl	23.1	4141	*exceeds phi*
	AB3, 170 MPa	997	2.12	39.2Px + 31.1Pl	27.7	4141	*exceeds phi*
	PRL entire	1014	3.50	20.2Px + 67.6Pl	12.2	4141	*exceeds phi*
	PRL 4-area med.	1014	3.50	86.9 Plag	13.1	4141	*exceeds phi*

Fig. 5-1 **Most relevant Viscosity model results:**

MELTS models: only basalt AB3 Liquid results shown here

All water content and Liquid compositions derived from MELTS models.

Liquid viscosity (non-Newtownian) calculated using equations of **Giordano et al. (2008)**. Viscosity is strongly influenced by water content.

Consistency of crystal suspensions (similar to viscosity) calculated using equations of **Moitra and Gonnermann (2014)** for randomly-packed unimodal distributions of large spheres (S-type = pyroxene) and small fibers (e-type = plagioclase), and bimodal distributions (Se-type).

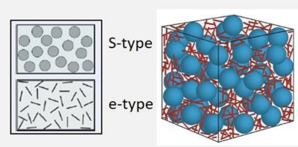

from M&G, 2014:
Left: Fig. 6b
Right: Fig. 19

Suspension crystallinity exceeds maximum for random packing (phi) after PLAG mantles form; coincides with PRL formation, PLAG alignment and cementation.

Calculated consistency values for random packing may differ significantly from PRL with aligned PLAG.

Figure 5-2: Chart showing how calculated viscosity (or consistency) increases as Temperature decreases in basaltic Liquid (no crystals) and magma with crystals up to PLAG mantle crystallization stage.

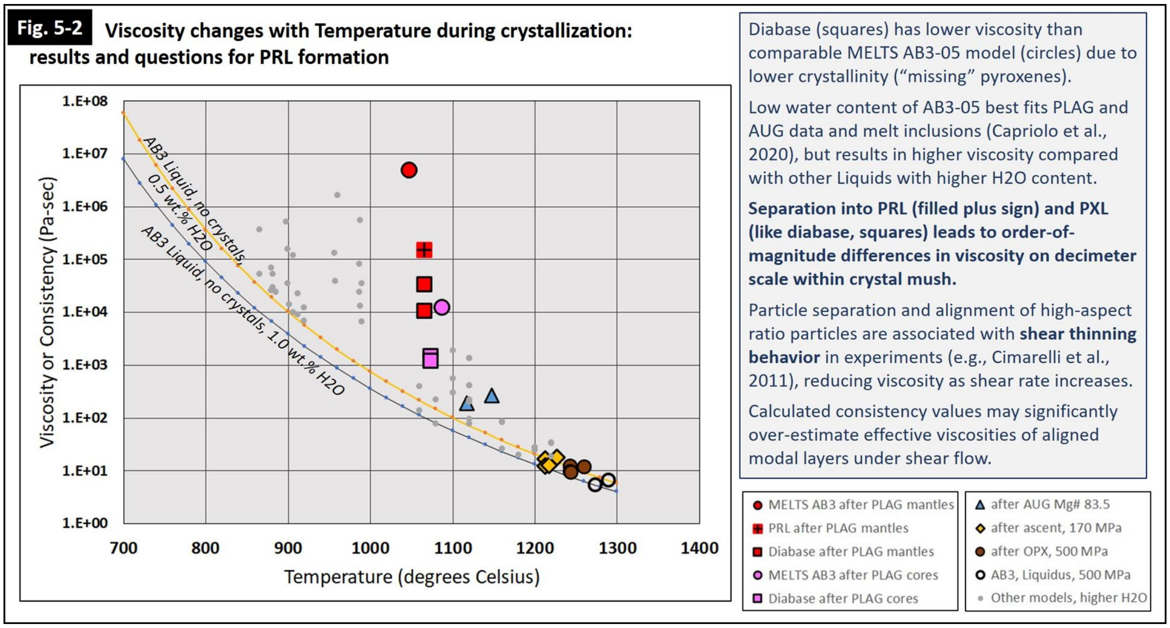

Figure 5-3: Macro-structures in the diabase quarry provide evidence for the general rheology of the mush after PRL formation. Initial stages: lateral sheet flow of later basaltic inputs into non-rigid but coherent layered mush.

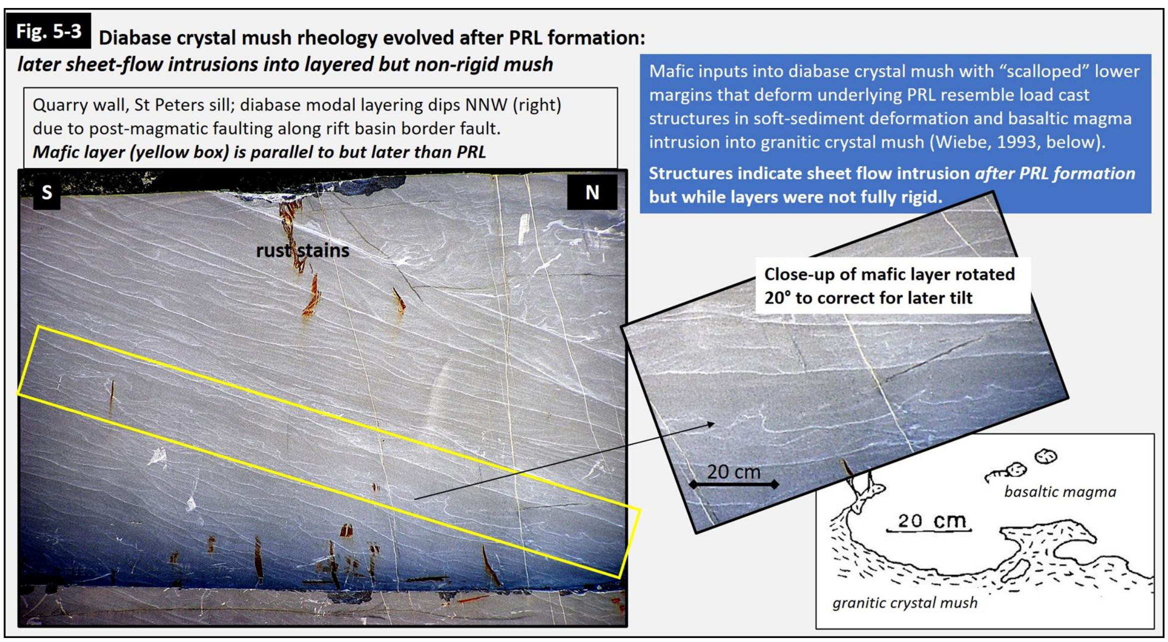

Figure 5-4: Later basaltic sheet cross-cuts more rigid layers and produces drag folds of the PRL in underlying crystal mush.

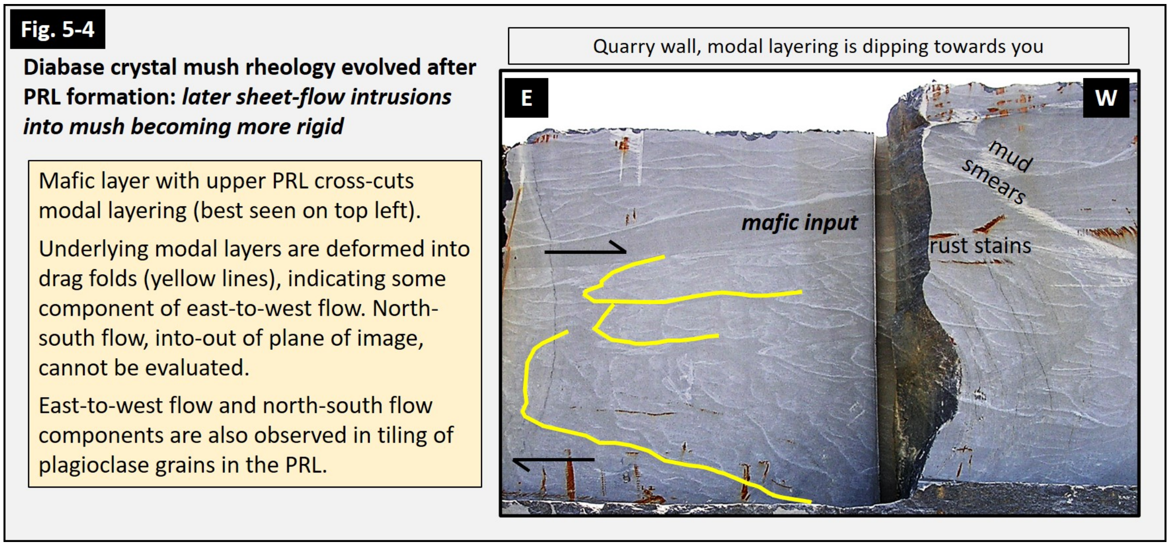

Figure 5-5: Channelized, vertical flow of late-stage basaltic inputs into diabase crystal mush with heterogeneous viscosity and rigidity. Is channelization a sign of decreasing magma flux? Did the mush rheology change the flow regime and prevent later basaltic inputs from rejuvenating the mush and leading to eruption?

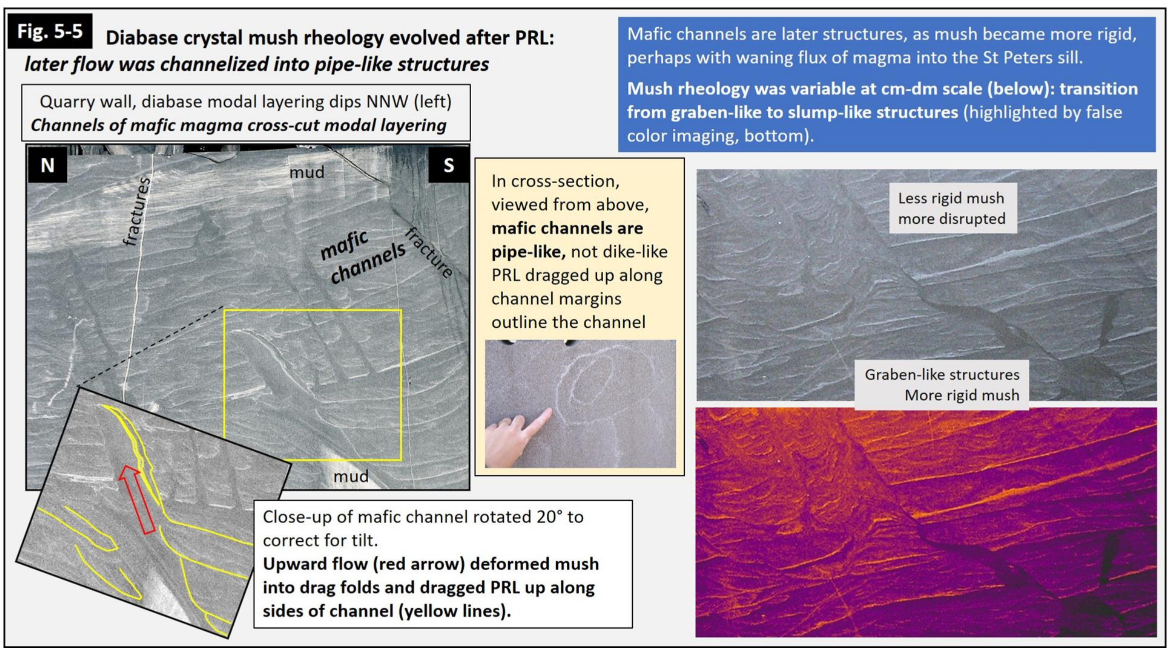

6. CONCLUSIONS

Summary: We propose a magma system chronology for crystallization in a sill-dike-basalt network in middle and upper crust (Figure 6-1). Three major findings are summarized below Figure 6-1.

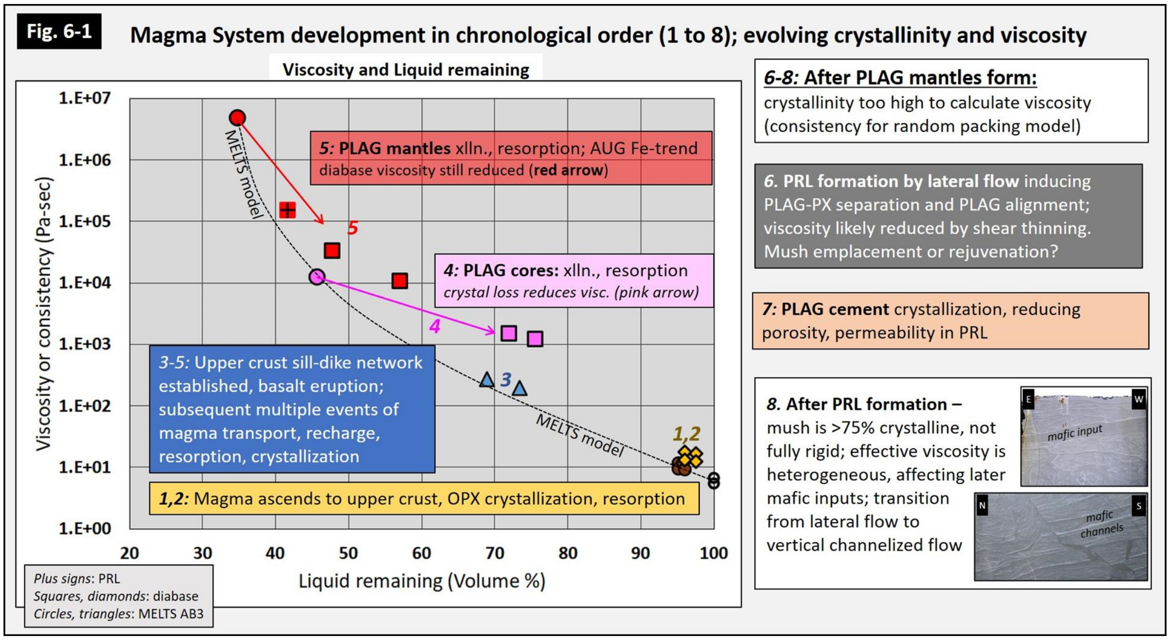

1) Recharge displaced mush and led to eruption of basalt with crystal cargo relatively early in system history, when crystallinity was 25-35% and viscosity 200-250 Pa-sec. Eruption did not require rejuvenation or mobilization of highly-crystalline mush.

2) Lateral magma flow during later emplacement or rejuvenation of mush in the St Peters sill led to self-organization of flow lobes with modal layering which likely reduced effective viscosity by shear thinning.

3) As the heterogeneous rheology of layered, high-viscosity mush evolved, the behavior of younger magma inputs into the St Peters sill changed from lateral flow to vertical channelized flow; this may have prevented mush rejuvenation and eruption in the last stages of the system history.

REFERENCES

Asimow, P. D., & Ghiorso, M. A. (1998). Algorithmic modifications extending MELTS to calculate subsolidus phase relations. American Mineralogist, 83, 1127-1131.

Blackburn, T. J., Olsen, P. E., Bowring, S. A., McLean, N. M., Kent, D. V., Puffer, J., McHone, G., Rasbury, E. T., & Et-Touhami, M. (2013). Zircon U-Pb geochronology links the end-Triassic extinction with the Central Atlantic Magmatic Province. Science, 340, 941-945.

Capriolo, M., Marzoli, A., Aradi, L. E., Callegaro, S., Dal Corso, J., Newton, R. J., Mills, B. J. W., Wignall, P. B., Bartoli, O., Baker, D. R., Youbi, N., Remusat, L., Spiess, R., & Szabo, C. (2020). Deep CO2 in the end-Triassic Central Atlantic Magmatic Province. Nature Communications, 11. https://doi.org/https://doi.org/10.1038/s41467-020-15325-6

Cimarelli, C., Costa, A., Mueller, S., & Mader, H. M. (2011). Rheology of magmas with bimodal crystal size and shape distributions: Insights from analog experiments. Geochemistry, Geophysics, Geosystems, 12(7). https://doi.org/10.1029/2011GC003606

Currier, R. M., & Marsh, B. D. (2015). Mapping real time growth of experimental laccoliths: The effect of solidification on the mechanics of magmatic intrusion. Journal of Volcanology and Geothermal Research, 302, 211-224.

Ghiorso, M. A., & Sack, R. O. (1995). Chemical Mass-Transfer in Magmatic Processes .4. A Revised and Internally Consistent Thermodynamic Model for the Interpolation and Extrapolation of Liquid-Solid Equilibria in Magmatic Systems at Elevated Temperatures and Pressures. Contributions to Mineralogy and Petrology, 119, 197-212.

Giordano, D., Russell, J. K., & Dingwell, D. B. (2008). Viscosity of magmatic liquids: A model. Earth and Planetary Science Letters, 271, 123-134.

Gualda, G. A. R., Ghiorso, M. S., Lemons, R. V., & Carley, T. L. (2012). Rhyolite-MELTS: A modified calibration of MELTS optimized for silica-rich, fluid-bearing magmatic systems. Journal of Petrology, 53, 875-890.

Lindsley, D. H. (1980). Pyroxene thermometry. American Mineralogist, 68, 477-493.

Marzoli, A., Jourdan, F., Puffer, J. H., Cuppone, T., Tanner, L. H., Weems, R. E., Bertrand, H., Cirilli, S., Bellieni, G., & De Min, A. (2011). Timing and duration of the Central Atlantic magmatic province in the Newark and Culpeper basins, eastern U.S.A. Lithos, 122, 175-188.

Marzoli, A., Renne, P. R., Piccirillo, E. M., Ernesto, M., Bellieni, G., & De Min, A. (1999). Extensive 200-million-year-old continental flood basalts of the Central Atlantic Magmatic Province. Science, 284, 616-618.

Moitra, P., & Gonnermann, H. M. (2015). Effects of crystal shape- and size-modality on magma rheology. Geochemistry, Geophysics, Geosystems, 16, 1-26. https://doi.org/doi:10.1002/2014GC005554

Neave, D. A., & Putirka, K. D. (2017). A new clinopyroxene-liquid barometer, and implications for magma storage pressures under Icelandic rift zones. American Mineralogist, 102, 777-794.

Putirka, K. (2008). Thermometers and barometers for volcanic systems. In K. Putirka & F. Tepley (Eds.), Minerals, Inclusions, and Volcanic Processes (pp. 61-120). Mineralogical Society of America. https://doi.org/DOI: 10.2138/rmg.2008.69.3

Srogi, L., Lutz, T., Dickson, L. D., Pollock, M., Gimson, K., & Lynde, N. (2010). Magmatic layering and intrusive plumbing in the Jurassic Morgantown Sheet, Central Atlantic Magmatic Province. In G. M. Fleeger & S. J. Whitmeyer (Eds.), The Mid-Atlantic Shore to the Appalachian Highlands: Field Trip Guidebook (pp. 51-68). Geological Society of America.

Srogi, L., Martinson, P. J., Willis, K. V., Lutz, T., Kulp, R., & Pollock, M. (2017). The 201-Ma magma plumbing system in the western Newark basin: how and (maybe) why it's different from the east. 34th annual meeting of the Geological Association of New Jersey, West Chester, Pennsylvania.

Watson, N., Srogi, L., Lutz, T., & Gimson, K. (2019). Textural study reveals dynamic development of mineral layering and crystal alignments by magmatic flow in a diabase sheet, western Newark Basin, Pennsylvania, USA [conference abstract]. annual national meeting, Geological Society of America, Phoenix, Arizona, USA.

Wiebe, R. A. (1993). Basaltic injections into floored silicic magma chambers. EOS, Transactions of the American Geophysical Union, 74(1), 1,3.

Willis, K. V., Srogi, L., Lutz, T., Monson, F. C., & Pollock, M. (2017). Phase composition maps integrate mineral compositions with rock textures from the micro-meter to the thin section scale. Computers and Geosciences, 109C, 162-177.